The Structure and Properties of Magnetron Sputtered Fe-Cr-Ni Coatings Containing Sigma Phase

Bertram Mallia, Karl L. Dahm, Abraham Ogwu, Peter A. Dearnley*

Fe-Cr-Ni alloy coatings were codeposited onto AISI 316L substrates using unbalanced magnetron sputtering. These were: (i) type B1, Fe-40Cr-4.5Ni; (ii) type B2, Fe-38Cr-8Ni; and (iii) type B3, Fe-55Cr-2.5Ni. In the as-deposited state, the B1 and B3 coatings mainly comprised solid solution α–$Fe_{(Cr)}$ and α'-$Cr_{(Fe)}$ phases, were fully dense, and had a microhardness of $\sim$700 kg $\cdot$ mm^{-2}, while coating B2 entirely comprised FeCrNi σ-phase, contained micro- or nanometre-scale porosity, and had a hardness of $\sim$370 kg $\cdot$ mm^{-2}. Despite being less hard, the as-deposited B2 coating displayed resistance to brittle fracture during scratch testing — this phenomenon was attributed to micropore toughening. When coating types B1 and B3 were partially or completely transformed to σ-phase (by vacuum heat treatment) brittle fracture took place during scratch testing.

Introduction

Austenitic stainless steels are used in the general and specialist engineering sectors where good corrosion resistance is required.[1] Unfortunately, these alloys are prone to galling and seizure in sliding contacts and display poor resistance to wear. Plasma surface engineering of austenitic stainless steels may provide a solution to this problem. Of the various possibilities, the application of thin hard coatings via magnetron sputtering, is attractive, provided that during use contact pressures remain below the yield strength of the substrate. Of the various coatings, *interstitial* materials like CrN and S-phase (a nitrogen supersaturated stainless steel), have received most investigation.[2] It is notable, however, that relatively little effort has been placed on investigating the potential of coating materials based on *intermetallic* compounds. The present work, reports on recent efforts to make coatings based on the intermetallic FeCrNi σ-phase. Since its first discovery by Bain and Griffiths, σ–phase has been regarded as something to avoid in monolithic steel structures as it can lead to severe embrittlement.[3] Although, σ-phase is known to be hard ($\sim$940 HV), its effect on corrosion behaviour is less clear. In one reported case,[4] the general aqueous corrosion resistance of duplex stainless steel was seen to be unaffected by the phase while localised corrosion resistance was impaired. In another paper,[5] σ-phase was found to improve the corrosive-wear behaviour of stainless steels.

The work reported here examines the feasibility of using unbalanced magnetron sputter deposition for synthesising coatings based on the Fe-Cr-Ni ternary system and evaluates procedures for stimulating the formation of σ-phase. The coatings were applied to AISI 316L substrates and characterised using a range of test procedures that included scratch testing. The latter enabled an assessment of fracture toughness during sliding contact.

B. Mallia, K. L. Dahm, P. A. Dearnley
School of Mechanical Engineering, The University of Leeds, Leeds LS2 9JT, UK
Fax: (+44) 113 3432150; E-mail: p.a.dearnley@leeds.ac.uk
A. Ogwu
Thin Films Centre, University of Paisley, Paisley, UK

Experimental Part

Sputter Deposition of Fe-Cr-Ni Coatings

A closed-field unbalanced magnetron deposition facility was used to codeposit the coatings. The unbalanced configuration produces

DOI: 10.1002/ppap.200730501

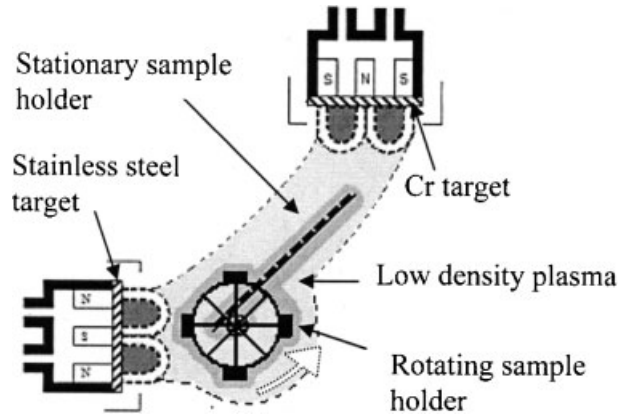

Figure 1. Schematic representation of the magnetron sputtering set-up.

a closed magnetic field that confines the plasma between the opposing cathodes and enhances substrate ion bombardment. The basic arrangement of the sputtering source of cathodes and the relative position of the substrates is shown in Figure 1. To establish basic coating deposition conditions, substrates were initially coated whilst being stationary. However, all the subsequent coatings were carried out using substrate rotation and it is the latter results that are reported and discussed here. Substrate rotation eliminates oblique sputtered matter flux and promotes dense uniform deposition. Table 1 summarises the processing parameters that were selected for pre-cleaning the substrates and applying the coatings on AISI316L and glass substrates. R.f. power was applied in order to induce a negative bias on the substrates. Cosputter deposition was carried out using 99.5% purity Cr and AISI 304L (Fe-19Cr-10Ni) austenitic stainless steel targets. This arrangement was found to yield coatings of preferable composition to enable the formation of σ-phase. When coatings were produced using an AISI 310 (Fe-25Cr-20Ni) target instead of AISI 304L, fewer coatings with σ-phase forming compositions were obtained. In the preferred arrangement, coating composition was changed by altering target current and voltage (coating types B1 and B3 in Table 1). The effect of varying substrate bias and chamber pressure was also investigated (coating B2), since it has been reported that varying deposition parameters can stimulate the formation of σ-phase.[6,7]

Heat Treatment

In order to produce more coatings containing σ-phase, several types of B1 and B2 coated AISI 316L test-pieces were heated in vacuum ($\sim 10^{-4}$ Pa) at 700 °C for 2 and 10 h using a Carbolite tube furnace. They were then transferred to a cold zone (without breaking the vacuum) and allowed to cool relatively rapidly to room temperature.

Characterisation of Coatings

Coating thickness and surface roughness were determined with the aid of a 2-D Form contacting Talysurf-120L profilometer set with a Gaussian cutoff filter of 0.8 mm and a bandwidth of 100:1. Surface roughness parameters (R_a and R_q) were measured in two perpendicular directions. To determine the coating thickness, surface regions were locally masked during deposition and then subsequently stripped to reveal a step. The height of each step was then determined by profilometry. Coating topography was also imaged directly using a combination of light optical microscopy (LOM; Leica) and scanning electron microscopy (SEM). The latter comprised a high resolution Hitachi S-4100 field emission gun SEM (FEG-SEM), an LEO-1530 FEG-SEM and an XL-30 Philips SEM. All were equipped with energy dispersive X-ray spectrometers (EDX) which were used to determine the coating composition. X-ray diffraction (XRD) was performed using Cu-K_α radiation under conventional Bragg–Brentano geometry (Bruker D8 and Siemens D500 diffractometers). Body centred cubic (bcc) crystal structures were identified by quantifying the ratios of the $\sin^2\theta$ reflections and comparing these with known quadratic forms of

Table 1. Sputter deposition parameters for Fe-Cr-Ni coatings.

Coating identification		**B1**	**B2**	**B3**
Substrate sputter cleaning phase	*Induced bias d.c. (V)*	−280	−290	−290
	Forward r.f. power (W)	200	200	200
	Chamber pressure (Pa)	1.33	1.33	1.33
	Duration (min)	60	60	60
	Chamber Gas	Ar	Ar	Ar
Deposition phase	*SS target current (A); Voltage (V)*	2; 475	2; 430	1.5;440
	Cr target current (A); Voltage (V)	2; 375	2; 330	3; 380
	Chamber pressure (Pa)	0.27	1.33	0.27
	Chamber Gas	Ar	Ar	Ar
	Substrate Induced d.c. (V)	−50	floating	−50
	Coating Duration (min)	190	190	190
	Substrate Rotation (rpm)	40	40	40

DOI: 10.1002/ppap.200730501

the Miller indices of this structure,[8] while σ-phase was detected by comparing the d-spacing data (corrected for systematic errors) by reference to the ICDD powder diffraction file no. 3-065-6712 (corresponding to the FeCr σ-phase, with unit cell dimensions of $a = b = 0.87966$ nm; $c = 0.45582$ nm and $a = \gamma = \beta = 90^{\circ}$).

Knoop microhardness tests were obtained using a Shimadzu HMV 2000 microhardness tester. Measurements were repeated five times. Scratch tests were performed using an adapted Zwick microhardness system fitted with a standard 250 μm tip radius Rockwell-C diamond stylus. Scratches were made at a sliding speed of 0.2 mm · s^{-1} using constant loads of 0.2, 0.5, 1, 2, 3 and 5 kg. The scratches were subsequently imaged and photographed using LOM.

Results And Discussion

Coating Composition and Basic Features

Coating compositions, determined by EDX, are shown in Table 2. Coating types B1 and B3 had the approximate weight percent compositions of Fe-40Cr-4.5Ni and Fe-55Cr-2.5Ni, respectively, while coatings of type B2 had the approximate composition of Fe-38Cr-8Ni. Since coatings B1 and B2 were deposited using identical target currents (Table 1), it is surprising that the Ni content was higher for B2 than B1 (Table 2). It is not clear why this happened although it is presumed that the higher processing pressure (1.33 Pa compared to 0.27 Pa used for B1) and floating bias conditions influenced this effect.

Coating B2 had a dark matt appearance, which SEM observation revealed to consist of dome-tipped asperities, separated by small gaps [Figure 2(a)]. There were also many near star shaped angular asperities that were ~2 μm across, as well as a number of flat elongated lath-like features. Coatings B1 and B3 had a shiny appearance that SEM observation revealed to comprise entirely of small acicular asperities whose main axis was ~1–2 μm long [Figure 2(b)]. The R_a and R_q values of the latter coatings were approximately half to one third of those of the B2 coatings (Table 3). Fracture cross-sections of the coatings deposited on glass revealed coating B2 to have a coarse columnar morphology [Figure 2(c)] that corresponded with Zone 1 of the Thornton classification system.[9] Some columnar porosity was also noted. Coatings B1 and B3, however, had a finer columnar morphology interspersed with some coarser columnar grains, indicating a mix of Thornton Zone 1 and Zone T morphologies [Figure 2(d)].

Coating thickness determinations (Table 2) showed that coating types B1 and B3 had similar growth rates, while that of coating type B2 was much greater. It is unlikely that more matter was deposited per unit time in the latter situation, even allowing for differing substrate bias and total chamber pressure conditions (Table 1). Rather, it is more probable, that the thicker B2 coating arose due to the incorporation of micro and nanometre scale porosity, as was suggested from coating topography [Figure 2(a)] and the Zone 1 growth morphology [Figure 2(c)].

XRD

As-deposited coating types B1 and B3 were found to comprise the bcc solid solution phases α-Fe$_{(Cr)}$ and α'-Cr$_{(Fe)}$, respectively, while coating B2 entirely comprised FeCrNi σ-phase (Figure 3). Vacuum heat treatment at 700 °C caused the B1 coatings to be completely transformed to σ-phase after only 2 h. However, the formation of σ-phase in the B3 coatings was much slower and only a partial transformation took place after 10 h heat treatment at the same temperature (Figure 3). The remainder of the heat treated B3 coating contained α'-Cr$_{(Fe)}$ phase. A further difference was that the heat treated B3 coatings contained σ-phase with a near random crystal orientation (indicated by the many different hkl reflections in Figure 3) whereas, the heat treated B1 coating had a σ-{002} preferred orientation indicated by a very intense diffraction peak. No other peaks were observed apart from the related lower order σ-{004} peak (Figure 3).

Table 2. Composition, phase constitution and thickness of Fe-Cr-Ni coatings.

Coating identification	Composition wt.-% obtained by EDX				Thickness	Phases identified by XRD		
	Fe	Cr	Ni	(Fe + Ni):Cr ratio	μm	As-deposited	700 °C, 2 h	700 °C, 10 h
B1	55.8	39.8	4.6	1.5:1	3.0	α–Fe$_{(Cr)}$ + σ (v. small)	σ	σ
B2	54.3	37.6	8.1	1.6:1	8.0	σ	Not heat treated	Not heat treated
B3	42.0	55.4	2.6	0.9:1	2.3	α'-Cr$_{(Fe)}$	α'-Cr$_{(Fe)}$ + σ (v. small)	σ + α'-Cr$_{(Fe)}$

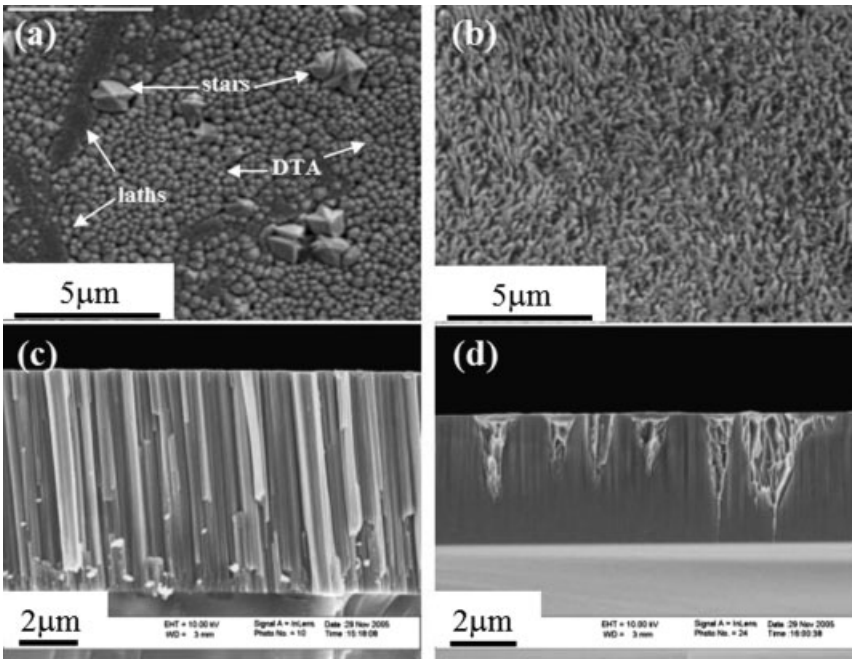

Figure 2. FEG-SEM images showing as-deposited morphologies of: (a) B2 coating surface, DTA = dome tipped asperities; (b) B3 coating surface; (c) B2 coating cross section; and (d) B3 coating cross-section.

Coating Hardness

The as-deposited coating types B1 and B3 had a Knoop microhardness of ~650 $kg \cdot mm^{-2}$ that increased only slightly (if at all) to ~700 $kg \cdot mm^{-2}$ when σ-phase was formed through heat treatment (Table 3). In contrast, as-deposited coating type B2, only had a Knoop microhardness of ~370 $kg \cdot mm^{-2}$. This is attributed to the coarse and porous columnar microstructure of this coating [Figure 2(c)]. When the B3 coating was heat treated at 700 °C for 2 h a slight reduction in Knoop microhardness from ~650 to ~600 $kg \cdot mm^{-2}$ took place (Table 3), even though some σ-phase was present (Figure 3). However, the latter phase was only a minor constituent of that particular coating and so the reduction in hardness can be attributed to a relaxation of the elastic microstrain of the α'-$Cr_{(Fe)}$ phase. This can be seen from the narrowing of the α'-$Cr_{(Fe)}$ {110} reflections (observed in the XRD diffractogram of the B3 coating after heat treatment at 700 °C for 2 h) compared to the broader {110} peak seen in the as-deposited condition (Figure 3).

Scratch Response of Coated AISI 316L

Even though scratch loads as high as 5 kg were deployed, there was no evidence of simple adhesive or cohesive failures of the coatings. However, other forms of degradation took place. During the plastic deformation of the substrate, two principal groups of *coating response* were observed: Group I plastic response of the coating and; Group II brittle response of the coating. The Group I features comprised:

F1. Plastically formed scratch groove without cracks
F2. Plastically formed shear lips without cracks

While, the Group II features comprised:

F3. Hertzian (circular) interlinked cracks at the position of scratch groove initiation.
F4. Radial cracks at the position of scratch groove initiation.
F5. High density craze cracks within the scratch groove.
F6. Plastically formed scratch groove containing cracks inclined at ~90° to the scratch direction.
F7. Cracks on shear lips inclined at ~45° to the scratch direction

Examples of these forms of degradation are collated in Figure 4, while an overview of the response of all the

Table 3. Surface roughness and hardness of Fe-Cr-Ni coated AISI 316L.

Coating	Roughness (as-deposited)		Roughness (700 °C, 10 h)		Knoop hardness (HK)		
	R_a, μm	R_q, μm	R_a, μm	R_q, μm	As-deposited	Heat treated 700 °C, 2 h	Heat treated 700 °C, 10 h
B1	0.030	0.036	0.034	0.041	653 ± 35	726 ± 28	677 ± 25
B2	0.061	0.081	Not applicable	Not applicable	371 ± 34	Not applicable	Not applicable
B3	0.021	0.027	0.048	0.061	657 ± 36	598 ± 48	700 ± 56

DOI: 10.1002/ppap.200730501

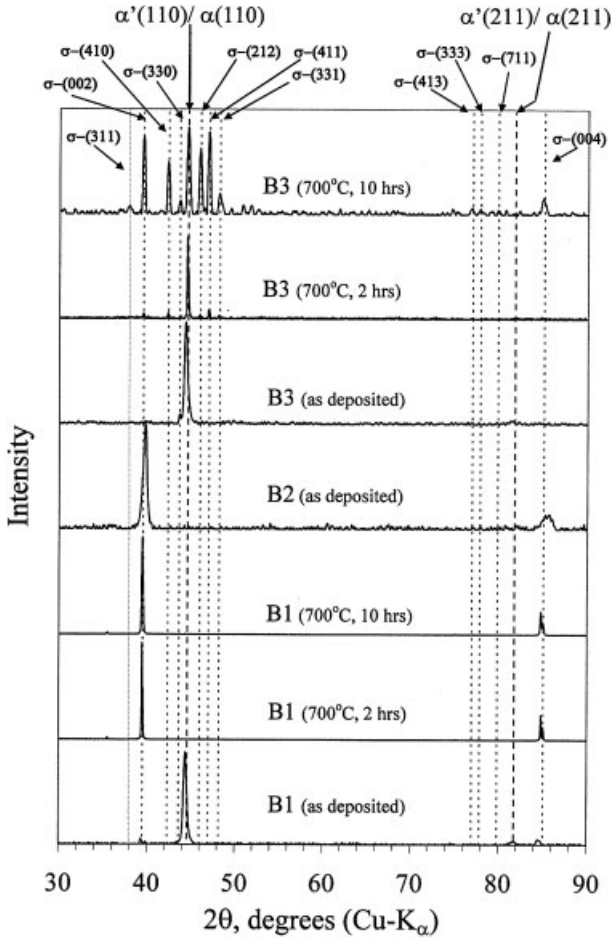

Figure 3. X-ray diffractograms obtained for type B coatings on AISI 316L substrates.

coatings to the scratch test is given in Table 4. Overall the tests indicated that the coatings *increased* in brittleness in the following sequence: as-deposited B1 ∼ as-deposited B3 → as-deposited B2 ∼ heat treated B3 (700 °C, 2 h) → heat treated B3 (700 °C, 10 h) → heat treated B1 (700 °C, 2 h) ∼ heat treated B1 (700 °C, 10 h).

The lack of fracture of the as-deposited coatings B1 and B3, indicated that the solid solution phases α-Fe$_{(Cr)}$ and α'-Cr$_{(Fe)}$, respectively, although hard (∼650HV; Table 3), were also tough. On the other hand, when coating B1 was heat treated at 700 °C for 2 or 10 h, the formation of σ-phase (Figure 3), resulted in a brittle response to scratch testing for both heat treated conditions (Table 4). On the other hand, coating type B3 (heat treated at 700 °C for 2 h) remained quite tough, since only a small quantity of σ-phase was produced, whilst the same coating material heat treated at 700 °C for 10 h resulted in a greater amount of σ-phase (Figure 3) and an accompanying increase in brittle behaviour (Table 4). However, the remaining α'-Cr$_{(Fe)}$ phase, in the latter coating, mitigated brittleness to some extent since the more severe F4 and F7 scratch modes were not observed.

The as-deposited coating B2, which mainly comprised σ-phase (Figure 3), was only slightly inferior in toughness compared to the B1 and B3 coatings (comprising α-Fe$_{(Cr)}$ and α'-Cr$_{(Fe)}$, respectively). This unexpected result suggests that micropores within the B2 coating, responsible for lowering hardness (Table 3), may have mitigated crack growth during scratch testing. A closely related and well-known phenomenon, is microcrack toughening.[10] This is widely observed in the fracture mechanics of monolithic ceramics like zirconia. The role of such spatial openings (pores or microcracks) is to cause the radius of a propagating crack tip to be enlarged, thereby lowering the magnitude of the stress (strain energy) in the matrix surrounding the crack, and so limiting further crack growth. Hence, the as-deposited B2 coating, probably displayed micropore toughening during scratch testing.

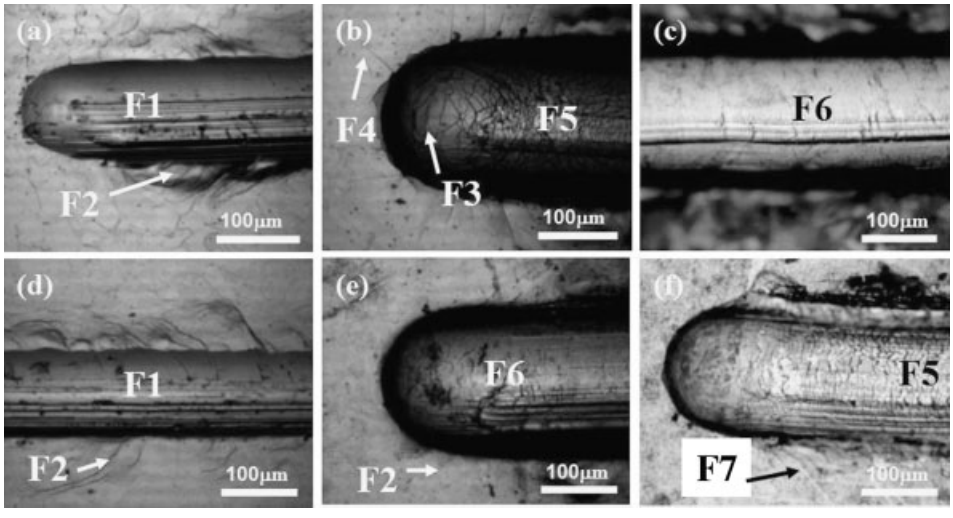

Figure 4. LOM images of scratches on (a) as-deposited B1 at 2 kg load; (b) heat treated B1 (700 °C, 2 h) at 5 kg load; (c) as-deposited B2 at 2 kg load; (d) as-deposited B3 at 2 kg load; (e) heat treated B3 (700 °C, 2 h) at 5 kg load; and (f) heat treated B3 (700 °C, 10 h) at 5 kg load. Scratch direction from left to right in all the cases. F codes explained in main text.

Table 4. Response of Fe-Ni-Cr coated AISI 316L to scratch testing (explanation of F codes given in the text).

Coating type	Scratch response	Relevant figure
As-deposited B1	F1 & F2 (all loads) →	Figure 4(a)
As-deposited B2	F1 & F6 at ≥0.5kg →	Figure 4(c)
As-deposited B3	F1 & F2 (all loads) →	Figure 4(d)
B1 heat treated at 700 °C for 2 hrs.	F6, F7 at 0.5 and 1.0 kg	
	F3, & F5 (≥2kg) →	Figure 4(b)
	F4 (5kg)	
B1 heat treated at 700 °C for 10 hrs.	F6 & F7 at 0.5 and 1.0 kg	
	F3 & F5 at ≥2kg)	
	F4 at 5kg	
B3 heat treated at 700 °C for 2 hrs.	F2 (all loads)	
	F6 at ≥1kg →	Figure 4(e)
B3 heat treated at 700 °C for 10 hrs.	F6 at ≥1kg	
	F5 at ≥3kg →	Figure 4(f)

Conclusion

Three coating compositions from the Fe-Cr-Ni ternary system were synthesised and applied to AISI 316L substrates by carrying out unbalanced magnetron sputtering of pure Cr and AISI 304L stainless steel targets:

1. In the as-deposited state, using a deposition pressure of 0.27 Pa and an induced bias of −50 V, two coatings with the approximate weight percent compositions of Fe-40Cr-4.5Ni and Fe-55Cr-2.5Ni (coded B1 and B3) were obtained by altering the target current. When using approximately the same target conditions as were used to obtain B1 coatings, and by increasing the deposition pressure from 0.27 to 1.33 Pa and using a floating self-bias, a coating with the approximate compositions of Fe-38Cr-8Ni (coded B2) was obtained.
2. In the as-deposited state the B1 and B3 coatings mainly comprised solid solution α-$Fe_{(Cr)}$ and α'-$Cr_{(Fe)}$ phases, respectively, while coating B2 entirely comprised FeCrNi σ-phase. While coatings B1 and B3 were dense, the B2 coatings contained micrometre and nanometre scale porosity. Vacuum heat treatment at 700 °C caused the B1 coatings to be completely transformed to σ-phase after only 2 h. However, the formation of σ-phase in the B3 coatings was much slower and a partial transformation took place after 10 h heat treatment at the same temperature. The remainder of this coating contained α'-$Cr_{(Fe)}$ phase. The σ-phase formed by vacuum heat treated coating type B1 showed a σ-{002} preferred orientation, while σ-phase produced by heat treated coating type B3, was near randomly oriented.
3. The as-deposited B1 and B3 coatings had a Knoop microhardness ∼650 $kg \cdot mm^{-2}$ that increased only slightly (if at all) to ∼700 $kg \cdot mm^{-2}$ upon forming σ-phase through heat treatment. The as-deposited B2 coatings were significantly lower in hardness (∼370 $kg \cdot mm^{-2}$) compared to the other coatings which was attributed to micrometre and nanometre scale porosity.
4. Scratch testing indicated that coatings *increased* in brittleness in the sequence: as-deposited B1∼as-deposited B3 → as-deposited B2 ∼ heat treated B3 (700 °C, 2 hrs) → heat treated B3 (700 °C, 10 h) → heat treated B1 (700 °C, 2 h) ∼ heat treated B1 (700 °C, 10 h). This indicated that the formation of σ-phase through heat treatment was detrimental to the toughness of the coatings.
5. Scratch testing of the as-deposited B2 coated AISI 316L samples indicated a slightly lower toughness compared to the as-deposited B1 and B3 coatings. However, they were much less brittle than the other σ-phase coatings. This behaviour was attributed to micropore toughening.

Acknowledgements: One author (P. A. D.) is indebted to *INTAS* for provision of research grant that supported aspects of the work reported here. Another author (B. M.) also thanks *The University of Malta* for a post-graduate research scholarship.

DOI: 10.1002/ppap.200730501

Received: September 15, 2006; Accepted: November 16, 2006; DOI: 10.1002/ppap.200730501

Keywords: intermetallic coatings; scratch test; sigma phase; toughness

[1] D. A. Jones, *"Principles and Prevention of Corrosion"*, 2nd edition, Prentice Hall, New Jersey 1996.
[2] P. A. Dearnley, G. Aldrich-Smith, *Wear* **2004**, *256/5,* 491.
[3] G. Krauss, *"Steels Heat Treatment and Process Principles"*, 4th edition, ASM International, Materials Park, Ohio 1995.
[4] J. H. Potgieter, *Br. Corrosion J.* **1992**, *27,* 219.
[5] X. Lu, S. Li, X. Jiang, *Wear* **2001**, *251,* 1234.
[6] E. D. Specht, P. D. Rack, A. Rar, G. M. Pharr, E. P. George, J. D. Fowlkes, XX. Hong, E. Karapetrova, *Thin Solid Films* **2005**, *493,* 307.
[7] M. Ohkoshi, *J. Appl. Phys.* **1988**, *63,* 2926.
[8] B. D. Cullity, *"Elements of X-ray Diffraction"*, 2nd edition, Addison-Wesley, London 1978.
[9] J. A. Thornton, *Ann. Rev. Mater. Sci.* **1977**, *7,* 239.
[10] T. H. Courtney, *"Mechanical Behaviour of Materials"*, McGraw-Hill, New York 1990.